Propagation of Shock Waves of Varying Curvature

S. Lewin and B. Skews[†]

Flow Research Unit, School of Mechanical, Industrial and Aeronautical Engineering, University of the Witwatersrand, Johannesburg, PO WITS 2050, South Africa.

†*Corresponding Author Email*: *beric.skews@wits.ac.za*

ABSTRACT

When a shock wave having variable concave curvature propagates, it can develop a kink followed by the development of a reflected shock. A typical example is a plane incident shock encountering a surface with concave curvature, the part of the shock adjacent to the surface curves forward and subsequently develops into a Mach reflection with a Mach stem, shear layer and reflected shock. The physical mechanisms associated with the evolution of the shock profile was evaluated for shock waves with initial profiles comprising a cylindrical arc, placed in-between two straight segments, propagating in a converging channel. The temporal variation of the pressure distribution immediately behind the shock wave was studied using CFD. This revealed a pressure imbalance in the region where the curved (which was initially cylindrical) and straight shock segments meet. This imbalance occurs due to the difference in the propagation behaviour of curved and planar shock waves, and results in the development of reflected shocks on the shock front. The angle at which the channel walls converge, the initial curvature radius, and the shock Mach number, was varied between 40 and 60 degrees, 130 and 190 mm and 1.1 to 1.4, respectively. The variation with time of the pressure-gradient distribution and the maximum pressure gradient behind theshock wave was evaluated. From this, the trajectory angle of the triple points, and the rate at which the reflected shocks develop, was deduced. It was found that when shock waves with larger curvature radii propagate in channels with lower wall angles, the reflected shocks develop at a slower rate, and the triple points follow a steeper trajectory. Consequently, the likelihood of reflected shocks emerging on the shock front, within the duration of the shock propagation, is reduced. This is due to the triple points intersecting the walls, before reflected shocks can fully develop. Similarly, when the shock Mach number is higher, the trajectory angle of the triple points is greater, and they intersect the walls before the reflected shocks can emerge.

Keywords: Curved shock waves; Shock diffraction; Shock reflection.

1. INTRODUCTION

When a cylindrical shock wave converges, it increases in strength (Payne 1957). This has been demonstrated experimentally by Perry and Kantrowitz (1951), and numerically by Sod (1977). A number of typical applications of shock waves with wave fronts concave in the direction of propagation has been given by Grönig (1986) . These works concentrate on cylindrically imploding shocks.

A general case is given in Skews *et al.* (2008), in an investigation into the generation of unsteady flows from rapidly moving boundaries. The contraction of a parabolic wall at a constant velocity produces a shock wave. The shock wave at distinct times during its motion is given in Fig. 1. The shock wave initially has the profile similar to that of the surface. It then develops kinks (second frame) with strong gradients

propagating out from the centre. In the final frame a three-wave system develops with a Mach stem and reflected wave.

A well known case is the propagation of a plane wave onto a concave surface as shown in Fig. 2. The compression waves arising from the curved surface, using the technique of generating small perturbations arising from tiny steps of the surface (Skews and Kleine 2009), shows the evolution of the shock profile. This illustrates how the compression behind the incident shock develops, resulting in its forward curvature due to its increasing strength. The top image shows how the compression wavelets congregate, bunching up causing a change in the curvature of the shock. In the second image some of the wavelets, but not all, combine causing the development of a kink in the shock. Those above and below the kink still continue to modify the shape of the section of the shock they interact with. In the final

image the central grouping of wavelets combine to form a reflected shock, forming a Mach reflection with its associated shear layer.
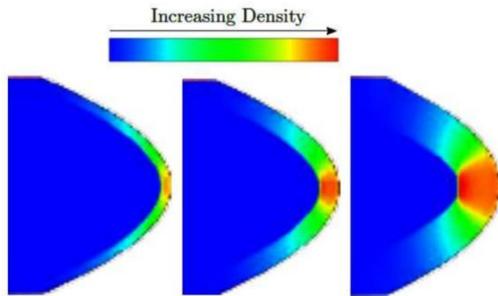

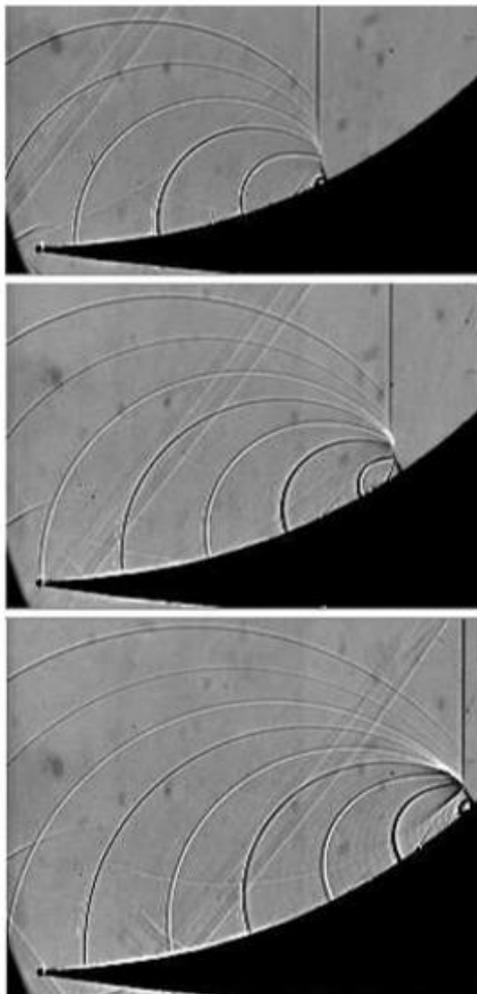**Fig. 1. Waves from a collapsing parabolic surface.**

Fig. 2. Modification of the profile of a shock wave on a curved surface due to influence of compression wavelets.

A third example arises from a suggestion in a doctoral project dealing with the reflection of cylindrical waves off a wedge (Gray 2014). This was part of a project dealing with the generation of twodimensional shocks of arbitrary profile. The

numerical results of one of the profiles that was suggested, are shown in Fig. 3. This profile comprises a cylindrical arc placed in-between two straight segments which are in a converging channel made up of a pair of straight converging walls. Initially, the shape of the shock wave resembles its original profile. Compression waves emanating behind the central region of the shock wave propagate outwards along the shock front and gradually coalesce. Immediately behind the shock front, this occurs in the region where the cylindrical and straight shock segments meet. As a result of the extent to which the compressions steepen two discontinuities in the form of kinks develop on the shock front. As the propagation of the shock wave progresses, two secondary shock waves eventually emerge from the kinks. The profile of the resulting shock wave has effectively transitioned from what was initially one curved shock wave, to a configuration which is a symmetrical pair of Mach reflections. The originally straight segments of the shock wave represent the incident wave (i), the cylindrical segment, the Mach stem (m), the secondary shocks being the reflected waves (r), and the kinks becoming, the triple points (t). The process on either side of the symmetry plane is very similar to that in Fig. 2.

All three of the above examples exhibit the same physical phenomena. In order to explore them the aim of the current investigation is to evaluate the physical mechanisms responsible for the development of reflected shocks on an initially smooth and continuous shock front. It uses the geometry of Fig. 3 to numerically investigate the effect of the initial curvature radius, shock Mach number and wall convergence angle on the characteristic aspects of the shock propagation.
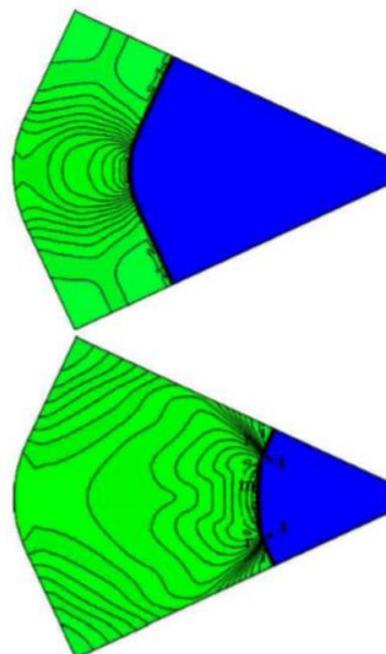

Fig. 3. Propagation of a compound shock wave.

2. NUMERICAL METHOD

The geometry of the computational domain was constructed with Autodesk Inventor, while ANSYS' Meshing and Fluent packages were used to generate the mesh and solve the governing equations of the flow. Post-processing of the subsequent results was performed with Tecplot 360, and scripts were written in MATLAB to analyse and generate plots of the relevant data. This section details how the flow was modeled and solved, and how the data required for analysis was obtained from the simulation.

2.1 Geometry

Due to the inherent symmetry of the geometry, it was only necessary to compute half the domain. A typical geometry is shown in Fig. 4. The left boundary was defined by the profile of the initial shock wave, which comprises a cylindrical arc and a straight segment. The straight segment is tangent to the cylindrical segment so that the composite profile is smooth and continuous. It is also normal to the walls of the propagation chamber. The length of the straight segment is thus determined by the length required to satisfy these conditions. The length of the computational domain was truncated. The radius of the cylindrical segment (referred to as the curvature radius of the shock wave) and the angle at which the chamber walls converge (referred to as the convergence angle of the walls) was varied in the different simulations.
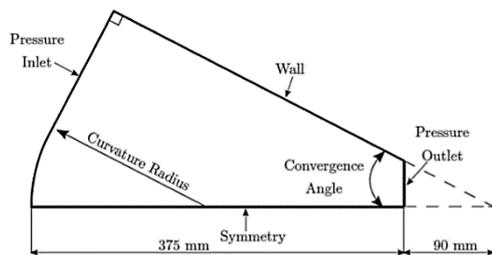
Fig. 4. Typical geometry of computational domain.

2.2 Mesh

To ensure that the curved surface at the inlet of the domain, (Fig. 4), was accurately represented, the initial mesh was generated based on curvature, with a curvature normal angle of 5 degrees, and a maximum cell size of 2 mm. It was also necessary to utilize adaptive mesh refinement during the simulations so that the shock wave was sufficiently resolved. Cells were marked for either refining or coarsening based on normalised gradients of pressure, density, temperature and velocity magnitude. Cells were refined up to four times if the normalised gradients were greater than 3% of the maximum and coarsened if the normalised gradients were less than 1.5% of the maximum. A typical adapted mesh is shown in Fig. 5.

2.3 Solver

The flow field under investigation contained shock waves so was analysed using ANSYS Fluent's density-based solver. The speed at which the solution converged, the memory requirements, as well as, solution accuracy, were considered when specifying the various settings of the density-based solver. The ideal settings were those which resulted in the fastest solution convergence and required the least memory, while simultaneously maintaining sufficient accuracy. As a result, the explicit formulation of the density-based solver was selected, with the Roe flux-difference splitting (Roe-FDS) and Least Squares Cell Based Spatial Discretization schemes. The first order implicit transient formulation was used, and the default Courant number (CFL) of 1 was retained. These settings provided the optimal combination of the afore-mentioned criteria.The size of the time step was determined so that the shock would be sufficiently resolved . A time step of 1×10^{-7} s was found to be appropriate. The air inside the domain was modelled as an inviscid, ideal gas and initialized with atmospheric conditions (pressure of 101325 Pa and temperature of 300 K). A shock wave was simulated at the pressure inlet boundary by specifying the conditions (static pressure, total pressure, total temperature) behind the shock wave of the desired strength.
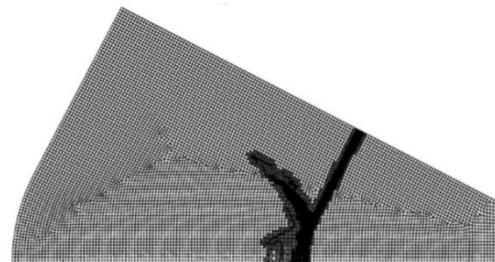
Fig. 5. Typical adapted mesh.

2.4 Extracting the Properties behind the Shock Wave

In order to provide a physical description of the shock propagation, it was necessary to obtain a temporal profile of the properties (specifically the pressure) immediately behind the shock wave. This required the nodes in the interior of the domain that represented the shock wave to be identified, so that the corresponding properties at these nodes could be exported into a suitable file for further analysis in MATLAB. The post-processing suite available in ANSYS Fluent allows cells with constant values of a specified variable to be distinguished and grouped together as a distinct surface. Since the shock wave was captured during the simulations with adaptive mesh refinement, it was possible to generate an isosurface representing the shock wave based on constant values of adaption space gradient. At each instant in time for which an analysis was required, the iso-value corresponding to the shock wave was selected interactively. As the iso-value was varied, an instantaneous preview of the corresponding isosurface was created. Superimposing this preview on a contour of the entire domain enabled an isovalue that accurately captured the shock wave to be determined.

Figure 6 demonstrates an example preview for one of the numerical simulations that was carried out. A preview of the surface corresponding to an isovalue of 0.05 is shown in Fig. 6a. In Fig. 6b, this is superimposed on a pressure contour of the domain, which shows that this specific iso-value corresponds to the shock wave. Once the shock wave was successfully detected, the properties (particularly the static pressure and x and y coordinates) at the iso-surface's constituent nodes were exported to an ASCII file. This file was then imported into MATLAB for further processing.

Since the shock is detected based on the property gradients across it, the iso-surface that is generated comprises two lines of nodes corresponding to the fluid immediately behind and in front of the shock wave. This is evident in the magnified view of the iso-surface in Fig. 6b. In order to evaluate the temporal variation of the properties of the fluid immediately behind the shock wave, it is the information at the corresponding line of nodes that is pertinent. As the fluid in front of the shock wave is undisturbed, the pressure at the corresponding line of nodes is atmospheric. Using this fact, the data at the line of nodes representing the fluid immediately behind the shock wave was distinguished for use in the subsequent analyses, by examining whether the static pressure at these nodes was significantly greater than atmospheric.
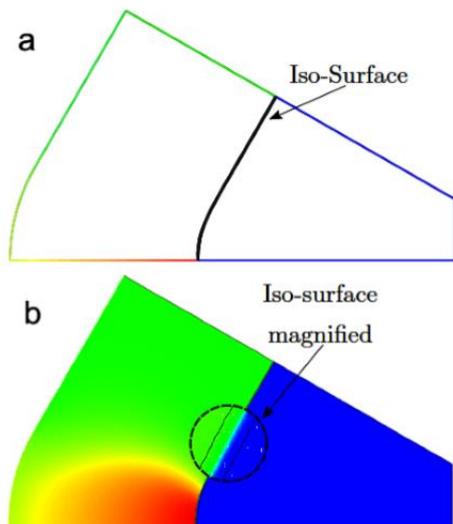

Fig. 6. Selection of a suitable iso-value. a: Preview of the iso-surface corresponding to an isovalue of 0.05. b: Iso-surface superimposed on pressure contour.

3. RESULTS

Simulations were run for a variety of independent variables. The angle at which the channel walls converged (Wall Convergence Angle), the initial Mach number and the initial curvature radius of the shock wave, ranged from 40 to 60 degrees, 1.1 to 1.4 and 130 to 190 mm, respectively.

The shock waves investigated have initial profiles comprising a cylindrical and straight segment. It will be shown that during the course of the shock propagation, the initially cylindrical shock segment is distorted, and hence, does not remain cylindrical. Thus, from here on, this portion of the shock will be referred to as the curved shock segment. Similarly, the straight section becomes slightly distorted, even though it appears straight in the figures presented. This is similar to the situation described when dealing with Fig. 2; the incident wave is almost always treated as being plane up to the triple point whereas it is actually influenced by compression waves arising above this point. Thus in the current study this segment will be identified as being nominally straight. The implications that the interaction of the curved and straight shock segments have on the phenomena that occur as the shock wave propagates in the channel is elucidated below.

3.1 General Description of Shock Propagation

The results for a typical case, in which the profile of the initial shock wave transitioned into a configuration resembling a symmetrical pair of Mach reflections, is shown in Fig.7. Pressure contours show the flow at different times from when the shock was at the inlet. Initially, the shock front is smooth and continuous. As the shock wave converges, the curved segment straightens, and two kinks develop on the shock front from which reflected shocks emerge. As the shock continues down the channel, the triple points of the Mach reflection pair follow a divergent trajectory towards the channel walls with increasing Mach stem length. Eventually, the reflected shocks and triple points meet the walls.

An evaluation of the pressure distribution immediately behind the shock wave demonstrates the mechanisms responsible for the phenomena depicted in the figure. For any time during the shock's progression, the x and y coordinates of the nodes representing the fluid immediately behind the shock wave, and the corresponding values of static pressure at those nodes, were obtained using the method described above. At any node, the length of the shock wave relative to the axis of symmetry was determined with numerical integration using the trapezoidal rule. It was then possible to plot the temporal variation of the pressure distribution along the length of the shock (Lshock). This is shown in

It is evident that throughout the duration of the shock's progression, the pressure distributions are analogous. For each curve, the distribution from the origin (which is at the axis of symmetry) to where the end of the shock wave meets the channel wall is obtained. The pressure is initially approximately constant up until some point, where there is a drop in the pressure. Beyond this region, the pressure is once again constant; until the weak compression waves reach the wall. Over time, the pressure increases before the pressure drop, while the pressure after it remains essentially constant. The increase in the slope of the curve at the pressure drop indicates that this drop becomes steeper with time.
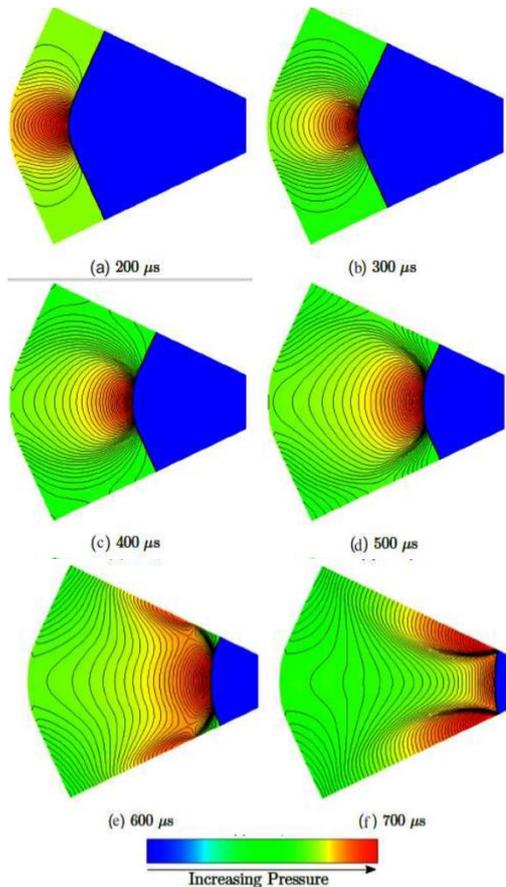
Fig. 7. Pressure contours for the propagation of a curved shock wave in a converging channel (Wall Convergence Angle: 50 Degrees; Initial Shock Mach Number: Mach 1.3; Initial Shock Curvature Radius: 160 mm).

Fig. 8 for the case portrayed in Fig. 7.

It is well-established, that the strength of planar shock waves is constant as they propagate. In contrast, cylindrical shock waves increase in strength as they converge. The pressure before the pressure drop, at the pressure drop, and after the pres-sure drop, corresponds to the pressure behind the curved shock segment, the region where the curved and straight shock segments meet, and the straight shock segment, respectively. The result of the pressure difference between these two regions manifests in the phenomenon shown in Fig 7. To adjust for this imbalance, compression waves, emanating from the region behind the curved segment, propagate outwards towards the region behind the straight segment. The effect of these compressions is to distort the shape of the curved shock segment, (this effect is discussed further later). As the strength of the curved shock segment increases as an imploding wave (and consequently, the pressured difference steepens), the strength of the subsequent compressions increases. As a result, they eventually coalesce into a pair of shock waves on the originally smooth shock front resulting in the configuration of a symmetrical pair of Mach reflections.
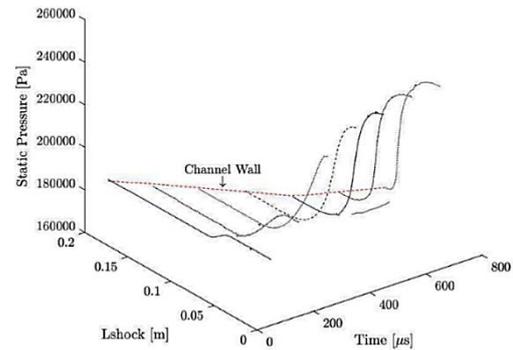

Fig. 8. Temporal profile of pressure distribution along the length of the curved shock wave (Wall Convergence Angle: 50 Degrees; Initial Shock Mach Number: Mach 1.3; Initial Shock Curvature Radius: 160 mm).

3.2 Influence of Critical Parameters

The initial Mach number and initial curvature radius of the shock wave, as well as the angle at which the walls of the propagation channel converge, are critical in determining how certain features of the shock evolution are manifested. The influence of these parameters on this process is discussed in the following sections.

3.21 Trajectory of Pressure Variations

The pressure distribution behind the shock wave was numerically differentiated using finite difference approximations. This gave the distribution of the pressure gradients along the length of the shock wave. The temporal variation of the pressure gradient distribution is shown in Fig. 9 for the case portrayed in Fig. 7.
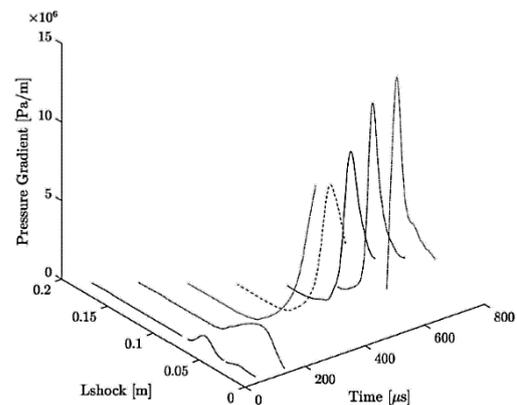

Fig. 9. Temporal profile of the pressure gradient distribution along the length of the curved shock wave (Wall Convergence Angle: 50 Degrees; Initial Shock Mach Number: Mach 1.3; Initial Shock Curvature Radius: 160 mm).

At any time during the shock's progression, the pressure gradient distribution is characterised by a rapid rise, followed almost immediately by a sharp dip in the pressure gradient. This occurs at some distance above the axis of symmetry (located at Lshock equals zero in Fig. 9), and is a consequence

of the pressure drop behind the shock wave (Fig. 8). The pressure drop behind the shock wave corresponds to the region behind the intersection of the curved and nominally straight shock segments. Therefore, here too, this rise and fall in the pressure gradient, and in particular, the pressure gradient peak, must correspond to this intersection.

As the shock progresses through the channel, the dip in the pressure gradient becomes steeper, and the pressure gradient peak increases. This is in accordance with the increase in the strength of the curved shock segment with time. The pressure gradient peak increases rapidly until some time, after which the increase is relatively gradual. The implications of this is discussed later.

It is apparent that the position behind the shock wave, at which the pressure gradient peak occurs, varies over time. Since this position corresponds to the region where the curved and nominally straight shock segments meet, it follows that by plotting the temporal variation of its position, the trajectory of this region can be obtained. This is shown in Fig. 10, where the position of the pressure gradient peak, represented by the filled circles, has been plotted on the shock wave at various times during its propagation.
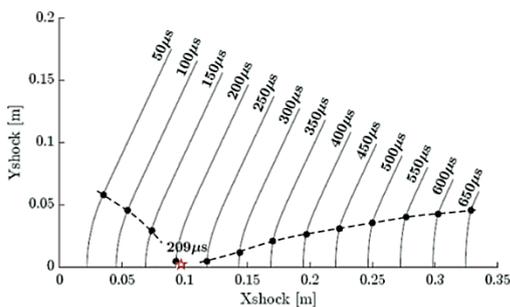

Fig. 10. Progression of a curved shock wave with an initial Mach number and curvature radius of 1.3 and 160 mm (Wall Convergence Angle: 50 Degrees).

At first, the pressure gradient peak moves towards the axis of symmetry (the x-axis in the figure), and then after reaching some minimum distance above it, it diverges away from the symmetry axis. Therefore, the propagation of the curved segment can be inferred from the trajectory of the pressure gradient peak. This conforms with what is known regarding the propagation of cylindrical shock waves; Initially, the curved segment (which was initially cylindrical) converges towards its focus, shown as a star, and then expands as it moves away from the focus. The minimum height that the pressure gradient peak reaches, before diverging away from the symmetry axis, must then be the apparent focus. The influence of the critical parameters on the trajectory of the pressure gradient peak (and by inference, the intersection of the curved and nominally straight shock segments), as the shock wave moves towards and away from the focus, is discussed below. The coordinates corresponding to the position of the pressure gradient peak over time were divided into

two sets; one representing the positions before the apparent focus, and the other representing the positions after focus.

3.22 Prior to Focus

The pressure gradient peak moves towards the plane of symmetry during this stage. Thus, even though there is some distortion of the circular profile with time, it still is an imploding curved wave strengthening as it propagates. The variation of the y-coordinate of the pressure gradient peak with time, and the time it takes for the shock wave to reach the focus was determined for all cases studied.

The variation of time to focus with the convergence angle of the channel walls, with different initial curvature radii and Mach numbers, is given in Fig. 11. Although there is some scatter in these plots, the dotted lines do capture the general trends. It is clear that when the angle at which the channel walls converge is greater, the time to focus is longer. It is also evident that when the initial curvature radius of the shock wave is larger, and the initial shock Mach number is lower, it takes longer for the shock to reach the focus. This result is in accordance with what one would expect, given that shock waves with larger curvature radii and lower Mach numbers are synonymous with weaker, and hence, slower shocks. angle. Left-hand plot: Mach number 1.1. Right-hand plot; initial radius 160 mm.

Intuitively, the rate at which the shock focuses (and consequently, the time to focus) is dependent on the rate at which the shock increases in strength before the focus. The Rate of Change (ROC) of the maximum pressure gradient over time is a convenient measure of the rate at which the shock increases in strength, and hence, of the acceleration of the shock wave. The rate at which the maximum pressure gradient changes with time before the focus is shown in Fig. 12 for the propagation of shock waves, with different initial Mach numbers and curvature radii, in channels with varying wall convergence angles. In all cases, at some time after the start of the shock propagation, there is an exponential growth in the rate at which the maximum pressure gradient increases, and hence, in the acceleration of the shock wave. Therefore, the earlier this increase occurs, the sooner the shock wave moves towards the focus. It is evident, that shock waves experience this exponential increase earlier, and therefore, arrive at the focus sooner, when the initial Mach number is higher, the initial curvature radius is smaller, and the wall convergence angle of the propagation channel is lower. This corresponds with the results presented in Fig. 11. Finally, the slope of the curves in Fig. 12a is steeper when the initial shock Mach number is higher. Therefore, the shock wave accelerates at a greater rate when the initial Mach number is higher. In contrast, the slopes of the curves in Fig. 12b and c are almost indistinguishable. This implies that the initial Mach number of the shock wave has a more significant influence on the rate at which the shock wave accelerates and reaches the focus than the initial curvature radius and wall convergence angle.
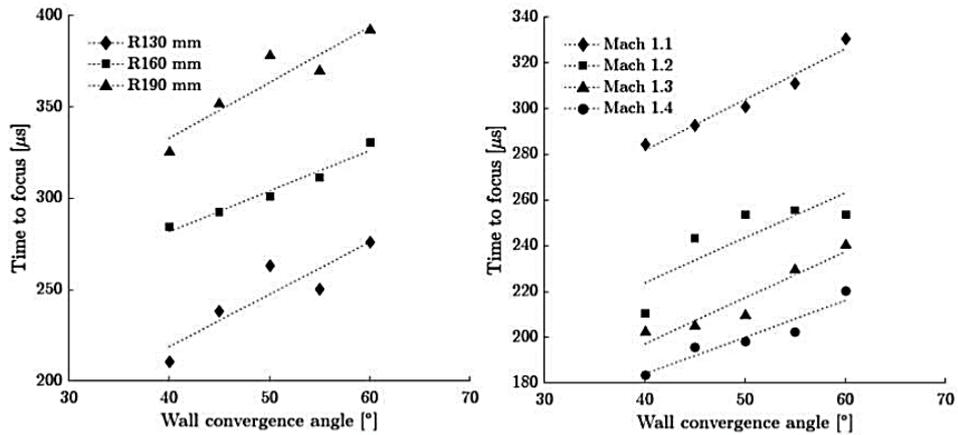
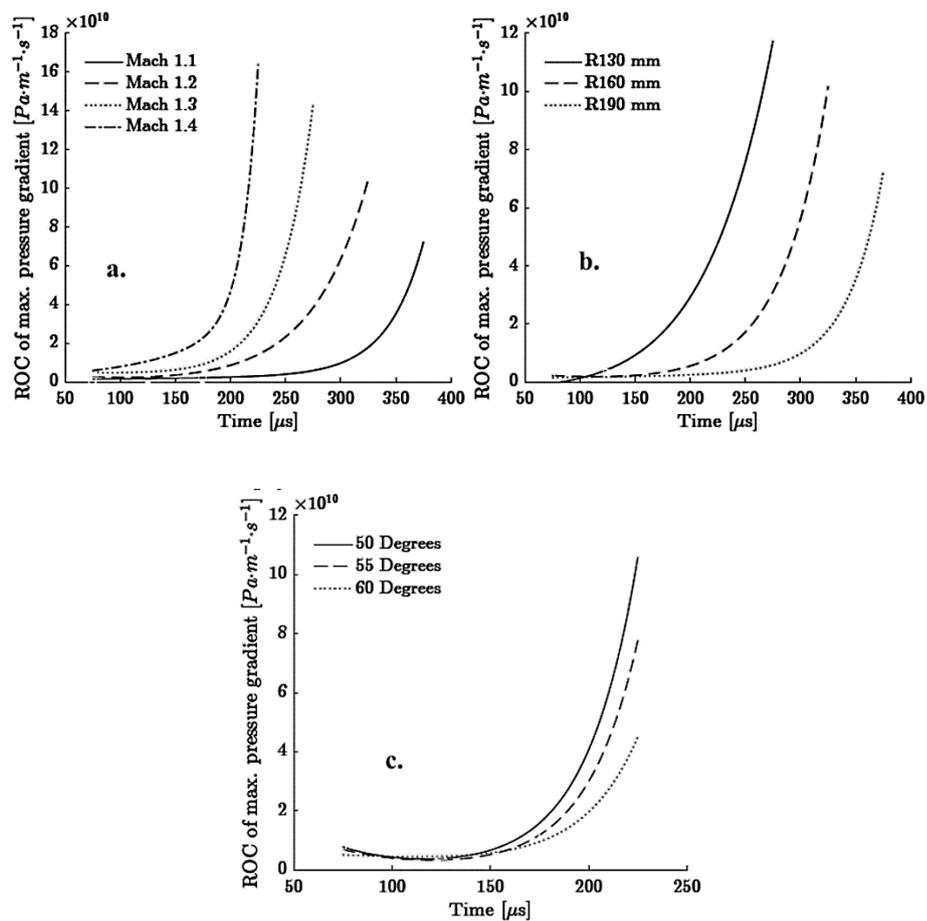**Fig. 11. Variation of time to focus with wall convergence.**

Fig. 12. Rate of change of maximum pressure gradient.

3.23 Post focus

For the case shown in Fig. 7 and 10 the apparent focus is at approximately $209\mu s$. Between 150 and 250 μs the curved wave has become increasingly distorted and considerably less cylindrical and no longer propagates as an imploding shock.

At this time, the reflected shocks have not yet developed. The dashed line on the left, plotted in Fig. 10, represents the initial propagation toward focus of the shock wave, and the line on the right (with the positive slope) corresponds to the trajectory of the peaks away from the focus. The pressure gradient peak behind the shock wave occurs in the region where the curved and nominally straight shock segments meet, and the subsequent drop in the pressure gradient becomes steeper with time (Fig. 9). As the drop in the pressure gradient becomes steeper, a discontinuity in the pressure behind the shock wave, in this region, begins to develop, as the

compression waves start to bunch together. This bunching together means less of the compression waves propagating ahead of the developing discontinuity affect the shock profile and therefore have less influence on its shape. Thus as the shock moves from $250\mu s$ to $600\mu s$ it becomes straighter aproaching the surface, as the curved portions contain the compressions eventually contributing to the reflected shock. This is analogous to the example in Fig. 2 where the more remote compressions do not contribute to forming the reflected shock. Since, discontinuities in the thermodynamic properties of a fluid are characteristic of shock waves, it follows that the reflected shocks eventually emerge in this bunched up region. Therefore, the upward sloping curve on the right in Fig. 10, not only describes the trajectory of this developing discontinuity region, and the development of a kink in the shock, away from the focus, it also represents the development of the trajectory of the triple points of the eventual Mach reflection pair. Thus, the slope of this line tends to that of the triple point trajectory.
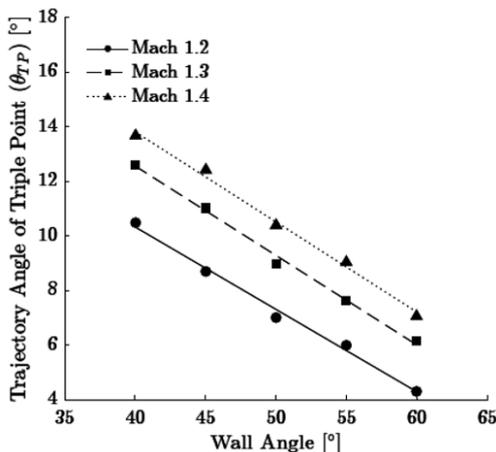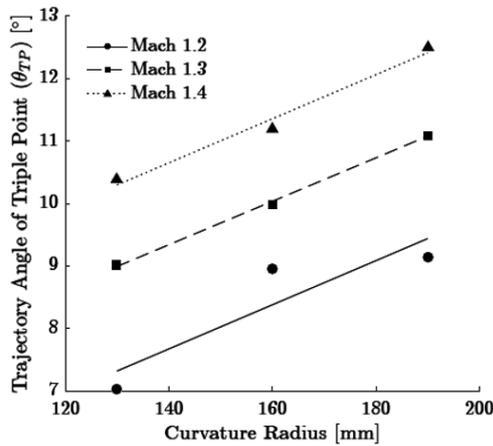

Fig. 13. Variation of the trajectory angle. Top: variation with initial curvature radius, wall angle 50°. Bottom: variation with wall angle, curvature radius 130 mm.

An approximate estimate of the trajectory is obtained by a linear fit to the data. The variation of the trajectory angle with the initial curvature radius and wall convergence angle, for shock waves with different initial Mach numbers, is given in Fig. 13. The higher the initial Mach number, the steeper the trajectory angle of the triple points. It is also steeper when the initial curvature radius of is larger, and the convergence angle of the channel walls is lower. Additionally, since the slopes of the different lines in the plots are almost identical, it can be inferred, that the rate at which the trajectory angle varies with the initial curvature radius and wall convergence angle is essentially independent of the shock Mach number.

3.3 Transition

In Fig. 14, the influence of the convergence angle of the channel walls, the initial shock Mach number, and the curvature radius, on the temporal variation of the pressure gradient distribution behind the shock wave is shown. The position behind the shock wave, where the pressure gradient peak and the subsequent drop in pressure gradient occurs, corresponds to where the reflected shocks eventually emerge. Thus, at any given time, the slope of the pressure gradient distribution at the drop is an indication of the degree to which the reflected shock has developed. Furthermore, the rate at which this slope becomes steeper over time indicates the rate at which the reflected shocks develop. Therefore, a comparison, at corresponding times, of the slope of the curves of the various cases in each plot allows the influence of the critical parameters on the rate at which the reflected shocks develop to be deduced.

Initially, the slope at the pressure gradient drop is steeper when the wall convergence angle is lower (Fig. 14a). This is because shock waves propagating in channels with lower wall angles converge to the focus at a faster rate. However, at later times during the shock's progression, the slope at the pressure gradient drop is steeper when the wall convergence angle is higher. The reason for this is that the strength of the shock wave (and accordingly, the magnitude of the maximum pressure gradient) when it arrives at the focus, is greater when the wall convergence angle is higher. Since the increase in the strength of the shock wave, as it moves away from the focus is gradual relative to the increase in its strength as it focuses, shock waves propagating in channels with higher wall convergence angles exceed in strength shock waves in channels with lower wall angles. Therefore, the rate at which the reflected shocks develop is greater when the wall convergence angle is higher. Hence, the reflected shocks emerge on the shock front earlier than when the wall angle is lower.

In Fig. 14b and Fig. 14c, it is evident that when the initial Mach number of the shock wave is higher, and the curvature radius is smaller, the slope at the pressure gradient drop becomes steeper at a greater rate. This is especially apparent at $200\mu s$ in Fig. 14b, and at $300\mu s$ in Fig. 14c. From this it can be inferred, that a reflected shock emerges on the shock front sooner when the initial Mach number of the shock wave is higher, and the curvature radius is smaller. In order to gain insight into the effect of the critical parameters on whether the profile of the shock wave

(a) Influence of wall convergence angle
(Initial Mach number: 1.1; Curvature radius: 160 mm)

(b) Influence of initial shock Mach number
(Curvature radius: 160 mm; Wall Angle: 50 °)

(c) Influence of curvature radius
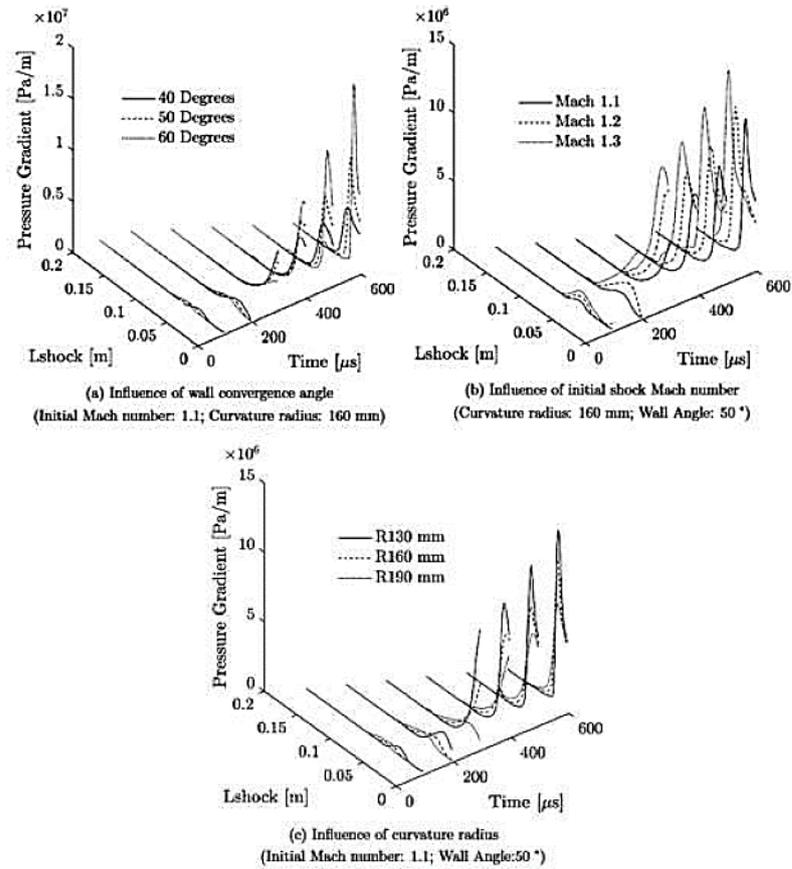(Initial Mach number: 1.1; Wall Angle:50 °)

Fig. 14. Temporal variation of the pressure gradient distribution behind the shock wave for different wall angles, shock Mach numbers, and curvature radii.

transitions within the duration of its propagation, the temporal evolution of the shock profile was evaluated. A shock wave was considered to have transitioned, if reflected shocks of comparable strength to the primary shock front had emerged before the region where the curved and nominally straight shock segments meet (representative of the locus of the eventual triple points), intersected the walls of the propagation channel.

In Figs. 15 to 17, pressure contours depicting the progression of the shock wave for different cases are shown, to illustrate how the various cases were assessed.

In Fig. 15, the shock wave, at $550\mu s$, is just prior to the instant the triple points meet the walls of the propagation channel (Fig. 15f). Although the compressions behind the shock wave have begun to coalesce into the start of reflected shocks, this has not occurred to the same extent as the compression of the primary shock wave. Therefore, in this case, it was considered that the shock wave had not yet transitioned before its triple points interacted with the channel walls. In contrast, in Fig. 16, even though the reflected shocks emerge only just before the triple points intersect the channel walls (Fig. 16f), the compressions have coalesced to a similar extent as those defining the primary shock wave. Thus, for this case, the shock wave was determined to have

(a) 50 μs

(b) 150 μs

(c) 250 μs

(d) 350 μs

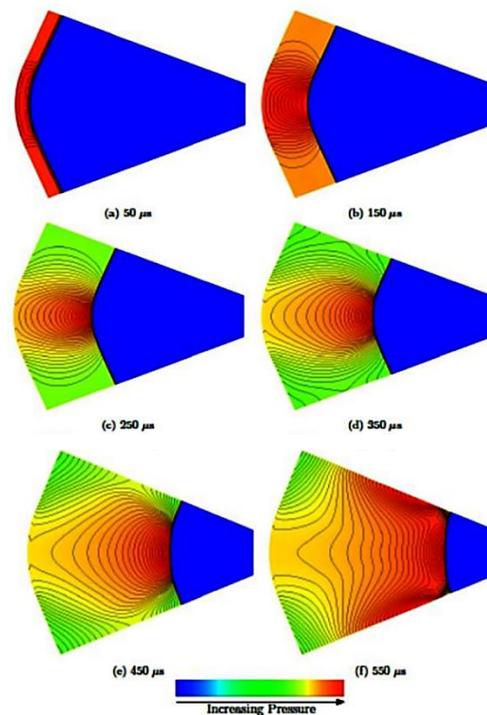(e) 450 μs

(f) 550 μs

Increasing Pressure

Fig. 15. Propagation of a shock wave in a channel converging at 45 degrees. The shock wave has an initial Mach number and curvature radius of 1.4 and 190 mm.

The transition classification of the various cases that were evaluated is presented in Fig. 18, for shock waves with initial curvature radii of 130 mm (coloured blue), 160 mm (coloured green) and 190 mm (coloured red). For each case, if the shock wave was determined to have transitioned, it was represented by a filled triangle in the figure. In the figure each distinct case can be identified by the initial Mach number of the shock wave (y-axis) and the wall convergence angle of the propagation channel (x-axis).

When the initial curvature radius was 130 mm, transition occurs for all wall angles and Mach numbers tested. However, where the initial curvature radius of the shock wave was 160 mm, when the convergence angle of the propagation channel was less than 45 degrees, and the shock Mach numbers was greater than 1.2, transition did not occur. Similarly, when the initial curvature radius is 190 mm, for wall angles less than 50 degrees and shock Mach numbers greater than 1.2, and for wall angles less than 45 degrees and shock Mach number greater than 1.1, transition does not occur.
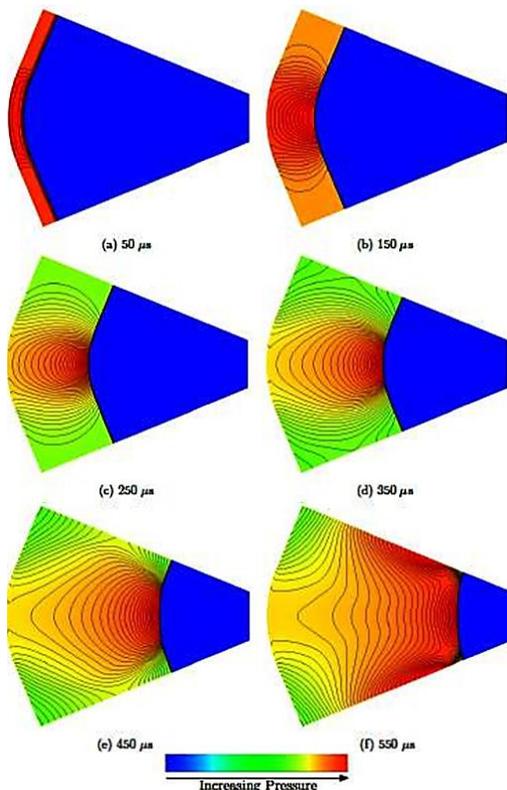

Fig. 16. Propagation of a shock wave in a channel converging at 50 degrees. The shock wave has an initial Mach number and curvature radius of 1.4 and 190 mm.

Although qualitative, the results of this evaluation do provide an indication of the influence of the critical parameters on transition. The likelihood of transition occurring during the shock's progression decreases when the initial Mach number and curvature radius of the shock wave is higher, and the convergence angle of the propagation channel is lower. This agrees with the earlier comments which showed that for the corresponding conditions, the trajectory angle of the triple points is greater. As was discussed there, when the trajectory angle of the triple points is greater, the triple points meet the walls of the channel earlier. Another aspect to consider is that when the initial curvature radius of the shock wave is larger and the wall convergence angle is lower, it takes longer for reflected shocks to develop. Consequently, for these conditions, the likelihood of transition occurring is reduced even further.
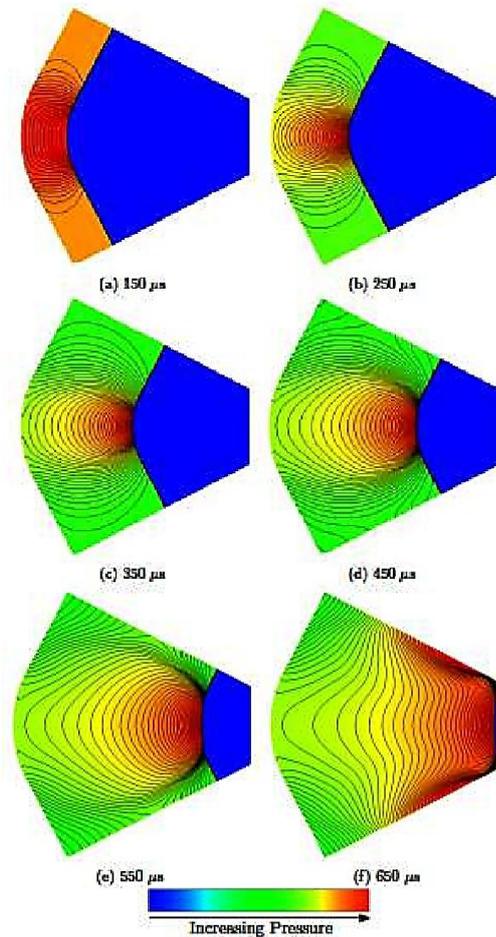

Fig. 17. Propagation of a shock wave in a channel converging at 55 degrees. The shock wave has an initial Mach number and curvature radius of 1.4 and 190 mm.

1. CONCLUSION

The propagation in a converging channel, of shock waves with initial profiles comprising a cylindrical arc in-between two straight segments was evaluated through various numerical simulations. The characteristic features of the change in the shock profile over the duration of its propagation were evaluated. In general, the curved segment of the shock front is distorted and flattened as the shock wave converges to its focus. As the shock propagates away from the focus, two kinks develop on the shock

front, from which reflected shocks emerge. This results in a configuration resembling a symmetrical pair of Mach reflections. The triple points of the Machreflection pair follow a divergent trajectory, away from the axis of symmetry.

The physical mechanism responsible for the development of the reflected shocks was elucidated by an evaluation of the temporal variation of the pressure distribution behind the shock wave. This showed that the pressure behind the curved shock segment increases over time, while the pressure behind the straight segments are essentially constant. Compressions propagate along the shock front towards the straight shock segments to correct this pressure imbalance. As the pressure behind the curved shock segment increases, subsequent compressions propagate at a greater velocity and eventually, they coalesce into reflected shocks. As a result of the increase in the pressure behind the curved shock segment with time, this portion of the shock front is distorted and flattened.
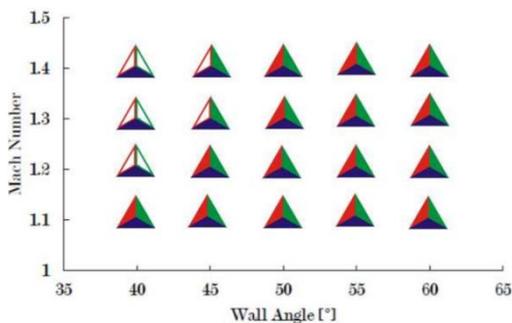

Fig. 18. Transition classification. Closed symbols represent development of Mach reflection. Initial curvature radius: Blue 130 mm; Green 160 mm: Red 190 mm.

The initial Mach number and curvature radius of the shock wave, as well as the wall angle of the converging channel was varied. It was found that: • When the wall convergence angle is lower, the initial curvature radius is smaller and the shock Mach number is higher, the shock wave moves towards focus sooner. The reason for this was that the rate at which the shock increases in strength, and hence accelerates, is greater. • When the wall convergence angle is lower, the initial curvature radius is larger, and the shock Mach number is higher, the trajectory

angle of the triple points is greater. As a result, the triple points intersect the walls of the channel earlier. The likelihood of reflected shocks developing within the duration of the shock's propagation in the channel is thus reduced. This effect is further exacerbated in cases where the wall convergence angle is lower and the initial curvature radius is larger since under these conditions, the rate at which the reflected shocks are formed is slower and therefore, the triple points intersect the channel walls before the reflected shocks can completely develop.

REFERENCES

Grönig, H. (1986). Shock wave focusing phenomena. In D. Bershader and R. Hanson (Eds.), *Proceedings of the fifteenth international symposium on shock waves and shock tubes*, Berkeley, CA, pp. 43–56. Stanford University Press.

Gray, B. (2014). *On the propagation and reflection of curved shock waves*. Ph. D. thesis, University of the Witwatersrand, Johannesburg, South Africa.

Payne, R. (1957). Numerical method for a converging cylindrical shock. *Journal of Fluid Mechanics* 2(2), 185–200.

Perry, R. and A. Kantrowitz (1951). The production and stability of converging shock waves. *Journal of Applied Physics* 22(7), 878–886.

Skews, B. and H. Kleine (2009). Unsteady flow diagnostics using weak perturbationsr. *Experiments in Fluids* 46, 65–76.

Skews, B., I. Komljenovic and T. Sprich (2008). Generation of unsteady flows from rapidly moving boundaries. In J. P. Meyer (Ed.), *6th International Conference on Heat Transfer, Fluid Dynamics and Thermodynamics*, Pretoria. HEFAT.

Sod, G. (1977). Numerical study of a converging cylindrical shock. *Journal of Fluid Mechanics* 83(4), 785–7946.